Numerical Simulation of Steel Moment-Resisting Frame Considering Panel Zone Yielding, Local Stiffening due to Bracing Connections, Beam Local Buckling and Fracture

LI Jionghui
Candidate for the Degree of Doctor of Engineering
Supervisor: Prof. OKAZAKI Taichiro
Division of Architectural and Structural Design

1. Introduction

Numerical simulation based on beam-column elements cooperated with fiber sections has been widely applied in structural analysis and design due to its high efficiency in computation. In Japan, moment-resisting frames (MRFs) are generally constructed by square hollow-structural-section (HSS) columns and I-section beams. Seismic behavior of panel zones in such columns is typically complicated by many factors, such as interaction of axial force and biaxial bending moments, stiffening from brace connections, and presence of composite slab, etc., and thus modeling of panel zone considering these factors is one of the challenges. Furthermore, steel MRFs subjected to extremely large or repeated earthquakes may suffer from beam local buckling and low-cycle fatigue. Significant losses of structural stiffness and strength usually accompany local buckling and low-cycle fatigue, which may result to excessive story deformation or even total collapse. Therefore, this study focuses on modeling schemes for steel MRFs taking account of panel-zone yielding, stiffening from brace connections, and beam local buckling and fracture, and examines how closely recorded responses of shake-table tests can be reproduced.

2. Shake-table tests on a 10-story specimen

Panel zone responses for this study were measured from shake-table tests on a nearly full-scale, 10-story steel MRF. Fig. 1 shows the dimensions of the specimen. The specimen was subjected to the 3D JMA Kobe motions (Kobe-NS to *Y*-direction, Kobe-EW to *X*-direction, and Kobe-UD to *Z*-direction), scaled from 25% to 100%. Yielding of the interior columns and column panel zones was expected from the relative proportions of the columns and beams. At grid point 2C, responses of such interior column, panel zones, BRBs and connecting beams were instrumented to understand the

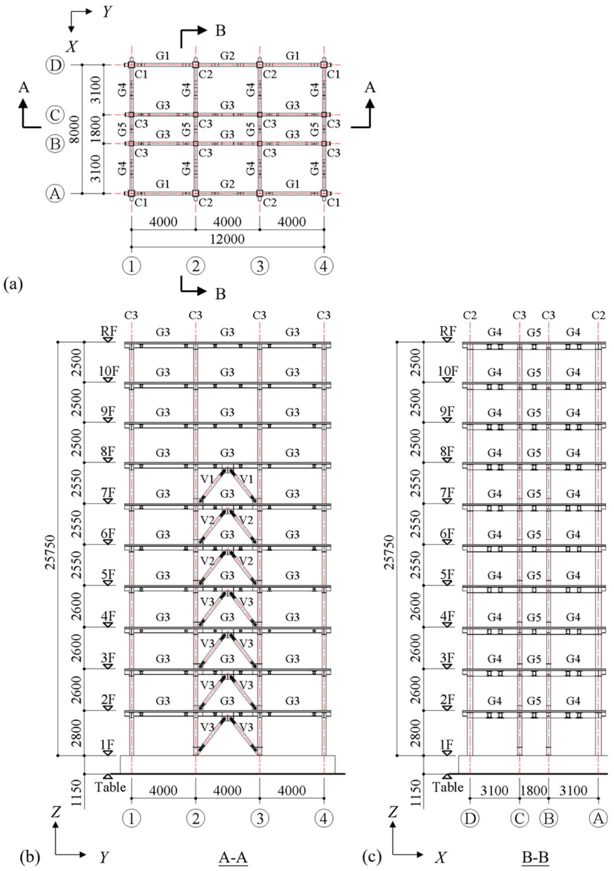

Fig. 1 Numerical model of 4-story specimen (unit: mm)

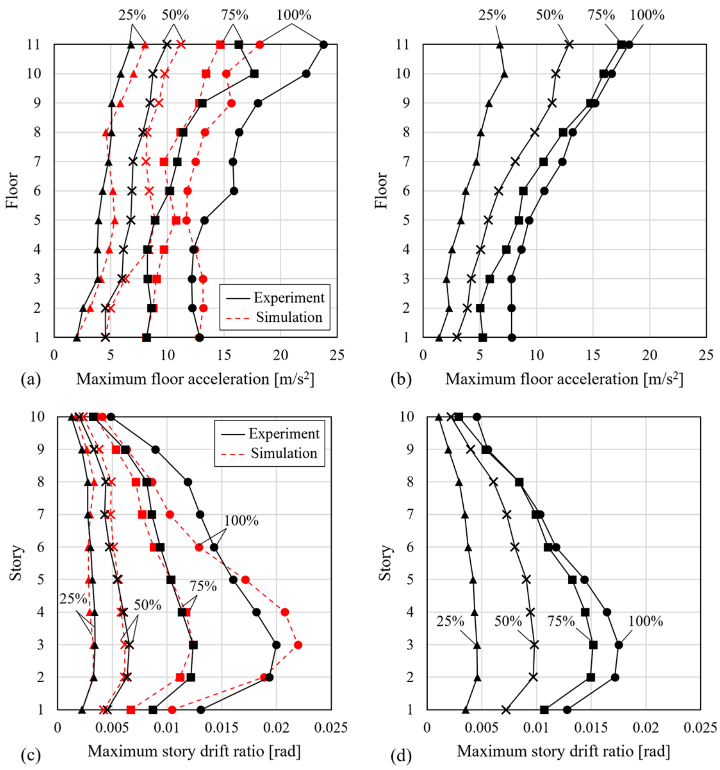

Fig. 2 Numerical model of 4-story specimen (unit: mm)

interaction among the members under combined cyclic loading. During the 100% JMA Kobe motion, the 10-story specimen yielded in the 1st to 8th stories developing maximum story drift ratio of 0.020 rad and 0.017 rad in the two orthogonal directions. Fig. 2 summarizes the maximum story drift ratios and maximum story shears for the *Y*- and *X*-direction. As expected, the columns and panel zones in the interior grid point yielded under biaxial forces, while the connecting beams remained elastic.

3. Shake-table tests on a 10-story specimen

Fig. 3 shows the processes to compute the panel-zone shear force in the X-direction. Positive bending moment (slab in compression) was decomposed using the method proposed by Kishiki et al. [1]. As shown in Fig. 3(b), positive bending moment was decomposed into bending moment developed in the steel section plus equal and opposite forces at the centroid of steel beam and composite slab, while the negative bending moment (slab in tension) was assumed to be taken by the steel section only. Fig. 3(c) shows the forces transferred to the panel zone converted to equivalent shear force, V_X.

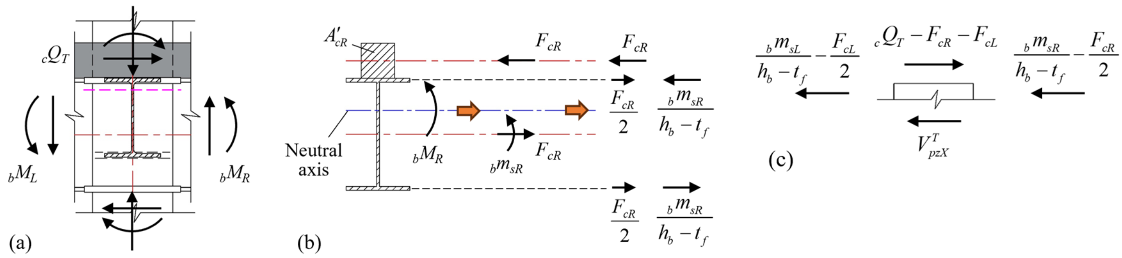

Fig 3. Panel zone-shear force in *X*-direction: (a) Component forces; (b) Decomposition of composite beam bending moment; (c) Shear force at top edge.

Fig. 4 shows the processes to compute the panel-zone shear force in the *Y*-direction. The BRB was assumed to deliver axial force only, and the horizontal component of the BRB force was assumed to be taken by the right beam only. Fig. 4(b) and (c) show how the forces in the beam and column segments stiffened by gusset plate were simplified. At the left end of the beam segment, normal stress was assumed to distribute linearly, and shear stress was assumed to distribute uniformly in the gusset plate and beam web. The column segment between the horizontal edge stiffener and upper diaphragm plate was subjected to forces from upper column and stresses from gusset plate, and the resultant forces at bottom were computed by equilibrium. Figs. 4(d) and (e) show the forces and stresses converted to equivalent shear force, V_Y.

Fig. 5(a) and (b) shows the *Y*- and *X*-responses of the panel zone at the 3rd floor measured during the 100% motion. The measured elastic stiffnesses agreed with the theoretical value K_v, which validated the described force deduction scheme. The panel zone showed notable plastic deformations in both directions. The maximum shear force in the *Y*-direction was lower than the plastic shear strength V_p per AIJ [2]. Fig. 5(c) shows the biaxial shear forces of the same panel zone normalized by V_p during the 100% motion, where the plastic limits was constructed using the plastic analysis method proposed by Arakida et al. [3]. Points A and B marked the times when the *X*-panel developed the maximum negative and positive deformations. At Point A, because of the large shear force developed in the *X*-direction, the plastic strength in *Y*-

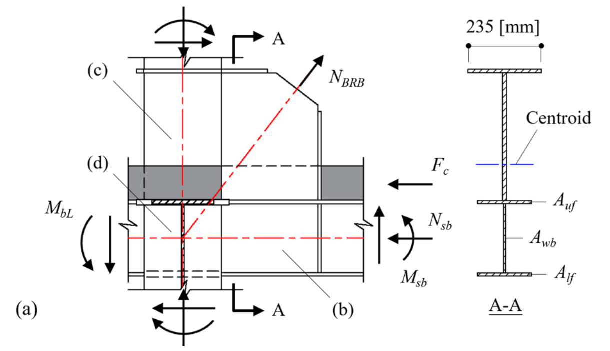

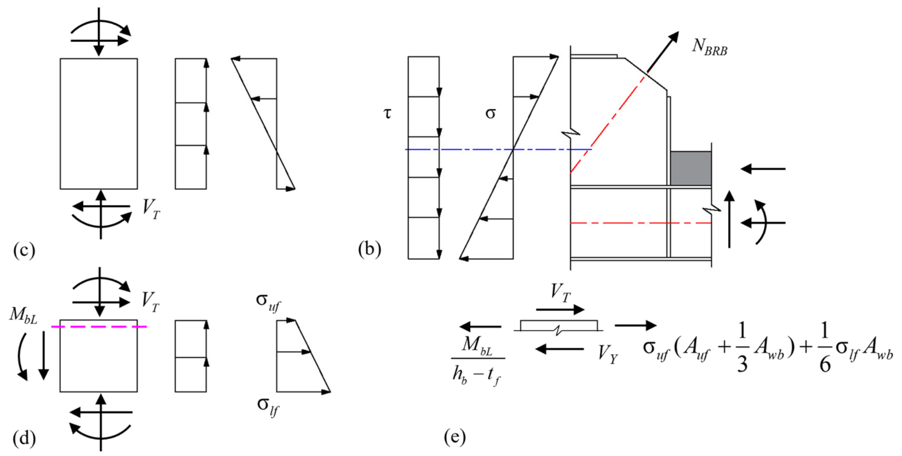

Fig. 4 Panel zone-shear force in Y-direction: (a) Component forces; (b) Beam segment; (c) Column segment; (d) Panel zone in Y-direction; (e) Panel-zone shear force in Y-direction.

direction decreased from V_p to $V_{pY,A}$ in Fig. 5, which might explain the Y-panel developed notable plasticity with shear force smaller than V_p. A similar behavior was observed at Point B.

4. Beam-to-column joint model stiffened by brace connections

A BRB-to-beam-to-column joint model was calibrated based on 2-D pushover analysis of a fishbone model (Luco et al. [4]) in the Y-direction. As shown in Fig. 6(a), the fishbone model consisted of Column 2C, half-length of the east and west beams, and the left BRBs. Fig. 6(b) shows the details of the joints. All panel zones adopted the modeling proposed by Gupta and Krawinkler [5]. At beam-to-column joints with BRBs connected, the gusset plate was simulated by an elastic steel truss with the same thickness as the gusset plate and width of a_{et} times the diagonal length l_{et}. The BRB was modeled by an elasto-plastic truss, two elastic beams and two rigid bars connected in series. The lower end of the BRB was rigidly connected to the panel zone. The columns and beams outside the joints were modeled by force-based beam-column elements with 6-point Gauss-Lobatto integration. Pushover analysis was conducted using the displacement measured from the 25% motion. Aspect ratio $a_{et} \geq$ 0.2 resulted in a good match of column inflection points at the 2nd to 4th stories between experiment and simulation. Time history analysis in the followed part adopted a_{et} = 0.2 to match the measured elasto-plastic panel zone response.

Fig. 6(c) shows the model comprising one exterior frame (Frame D) and one interior frame (Frame C) for time history analysis. Rigid trusses were assigned between Frames D and C at each floor to simulate rigid floor diaphragms. The same modeling schemes as in the pushover analysis were adopted. Rayleigh damping with a critical damping ratio of 0.02 was assigned to the 1st and 3rd natural periods. Analysis was executed continuously using the measured 25%, 50%, 75% and 100% table motions. The simulated responses are plotted in Fig. 2 against the measured responses. The model reproduced the measured story drift ratio with a good precision. Fig. 7 compares the simulated and measured response of the panel zone of Column 2C at the 3rd floor during the 100% motion. The simulated response agreed with the expected elastic stiffness and measured plastic deformation, but the simulated shear force was somewhat larger and the shear deformation was smaller than measured, presumably because the model did not consider strength reduction due to force interaction.

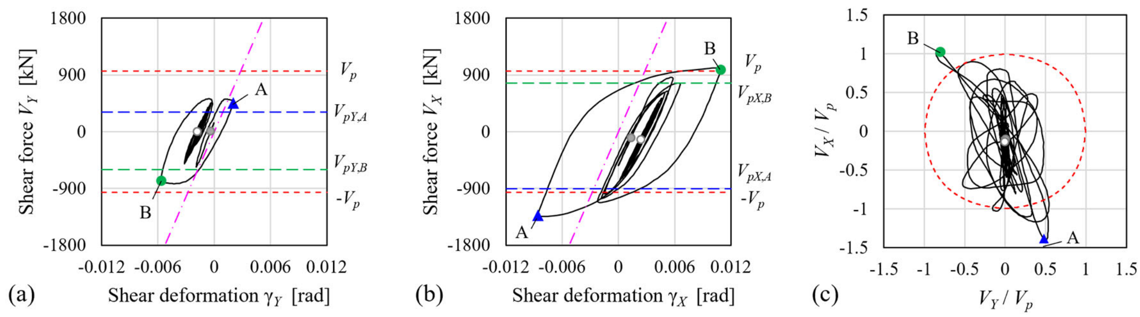

Fig 5. Panel zone responses in 100% motion: (a) Y-direction; (b) X-direction; (c) Biaxial shear force.

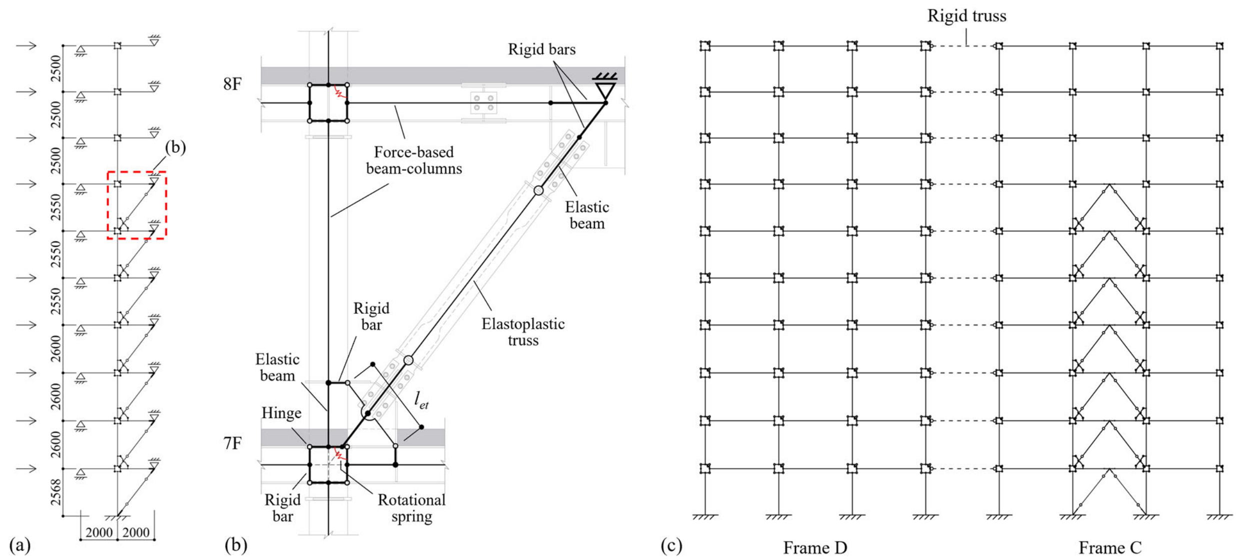

Fig 6. Simulation of 10-story specimen: (a) Pushover analysis; (b) BRB-to-Beam-to-Column model; (c) Time history analysis.

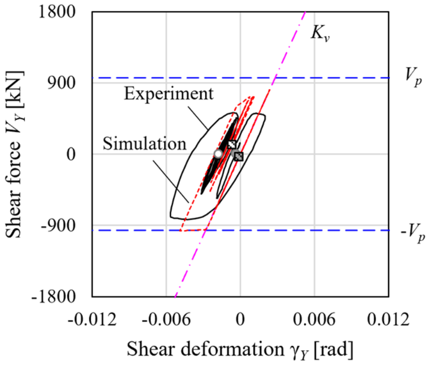

Fig 7. Simulated panel-zone responses

5. Simulation of beam local buckling and fracture

Local buckling of beams was simulated by the *Hysteretic* material model in OpenSees. Fig. 8 shows the backbone curve of the *Hysteretic* model, which adopted a bilinear model in tension and a trilinear model with degradation in compression. Low-cycle fatigue of beams was simulated by the *Fatigue* material in OpenSees [6], of which the fatigue limits based on a linear cumulative damage rule. Fig. 9(a) shows the Coffin-Manson relationship in log-log space, where the ε in vertical axis is constant strain amplitude and N_f is the number of cycles that material can sustain in that amplitude, where log(ε) is related to log(N_f) through intercept log(ε_0) and slope *m*. Damage accumulates with cyclic loading, and after the cumulative damage factor reaches 1, fiber stress is drops to zero. Fig. 9(b) shows the fiber section for the quarter beams and the fatigue parameters to be calibrated. From the shake-table tests and subassemblage test, fracture initiated at the edge of the beam flange near the CJP groove weld, and subsequently propagated through the flange and finally into the web. Therefore, ε_0 of the Coffin-Manson relationship was taken smaller at the flange edge, as $\varepsilon_{0,min}$, and larger by factor n_{sf} at the middle of flange, with a parabolic transition. At the beam web, the same value as the middle of flange was assigned.

The above material models were calibrated by cyclic loading tests on beam-and-column subassemblages extracted from a 1:2.5-scaled, 4-story steel MRF. Fig. 10 shows the numerical model for calibration, which represents one of the subassemblages. The beam was separated into two parts: the segment between the beam end and quarter point was modeled by a force-based beam-column element with 4-point Gauss-Lobatto integration, and the segment between the quarter point and inflection point was modeled by an elastic beam-column element.

Hardening ratio b_1 of the Hysteretic model was determined by a cyclic coupon test on steel of JIS grade SS400. Because crack happened and propagated at beam upper flange, parameters related to local buckling were calibrated by matching the response in the third quadrant (upper flange in compression) to the first ratcheting excursion from -0.05 to -0.125 rad before fracture happened. The parameters of the specimen shown in Fig. 10 were determined as ε_{cp} = -0.0135, b_2 = -0.0024E_s.

The fatigue parameters were determined to match the gradual degradation in measured stiffness and strength as well as observed crack propagation in the asymmetric loading excursions of 0 to -0.125 rad. Figs. 11 compares the experimental and simulated responses where the latter adopted the final parameters including $\varepsilon_{0,e}$ = 0.24 and n_{sf} = 2. The simulation traced the measured degradation beyond the range shown in Fig. 7(a). Fig. 8 compares the crack propagation in the upper flange observed from test against stress distribution obtained from simulation. The stages when crack in the beam flange propagated to 25%, 50%, 75% and 100% of the flange width are marked by A, B, C and D in Fig. 7(b), with subscript 'e' for experiment and 's' for simulation. Fig. 12 compares the simulated fiber failure and crack propagation in the test. Because the 2D model enforces symmetric behavior with respect to the minor axis of the beam section, simulation

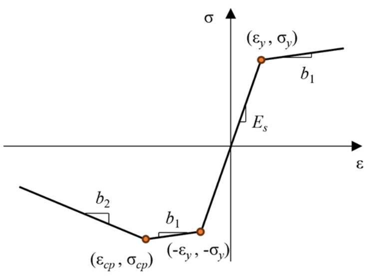

Fig 8. Backbone curve of Hysteretic model

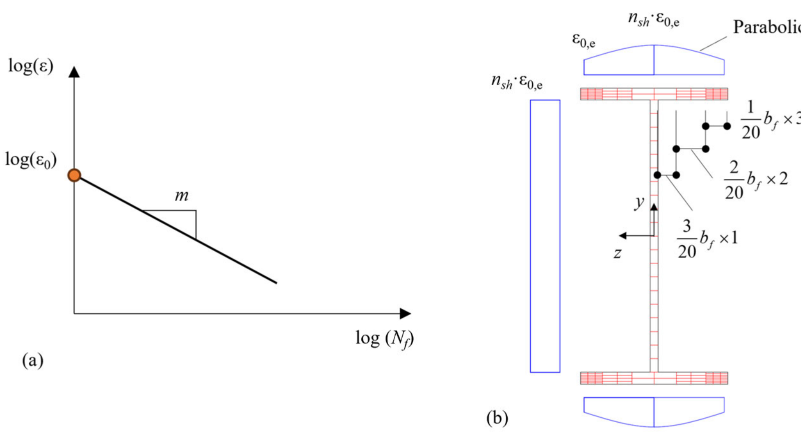

Fig 9. Fatigue model: (a) Coffin-Manson relationship; (b) Beam fiber section.

traced cracks occurring and extending simultaneously from the outer edges of the beam flange. Otherwise, the initiation and propagation of the simulated crack nicely matched the experimental observation.

6. Time history analysis of a 4-story specimen

To verify how closely the proposed modeling scheme can reproduce the responses measured from shake-table tests. A numerical model was built in OpenSees to simulate shake-table tests on a 1:2.5-scaled, 4-story steel MRF conducted in 2021. Fig. 13 shows the numerical model, which consisted of a MRF and a gravity frame. The horizontal degree of freedom of each pair of quarter points at the MRF and gravity frame were constrained to simulate rigid floor diaphragm. The beams of the MRF adopted the same modeling scheme as the calibration. Gravity load of each floor was distributed to the quarters nodes of the MRF and gravity frame according to the tributary area, and the floor mass was evenly assigned to the quarter points of the MRF only. The 4-story model was subjected to the measured excitations JMA Kobe-NS from 10 to 100%, where the 100% motions were conducted for 4 times.

Fig. 14 compares the simulated and measured maximum story drift ratio during the 50%, 100%-1, 100%-3 and 100%-4 motions. The simulated maximum story drift ratio underestimated the experiment since 100%-1 motion, presumably because ideal constrains were applied to the column bases of the model, while rotations of column bases were observed from the test.

Fig. 15 compares the bending moment and rotation of the exterior right beam end at the 2nd floor. Bottom flange of this beam end fractured during the 100%-3 motion in the test. The simulation successfully reproduced fracture at beam bottom flange and resulted to an obvious decrease of bending moment. The simulated elastic stiffness after fracture was also consistent with the measured value.

7. Conclusions

Panel zone responses were measured from shake-table tests of a nearly full-scale, 10-story steel MRF with BRBs. Method to derive panel-zone shear force was proposed, and a plastic

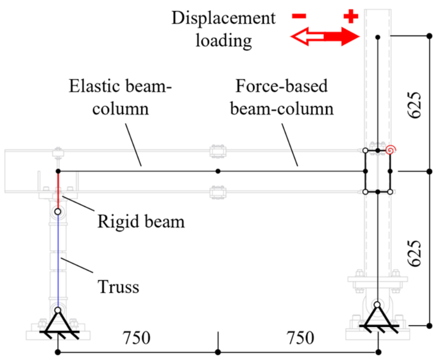

Fig 10. Subassemblage model for calibration

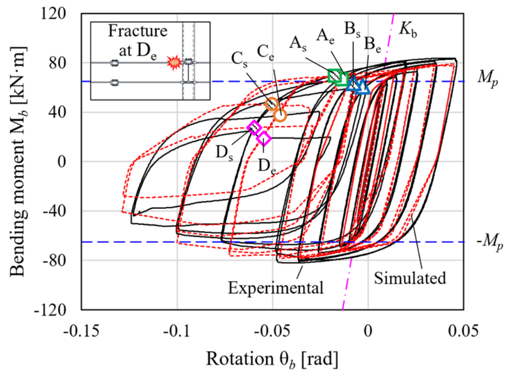

Fig 11. Backbone curve of Hysteretic model

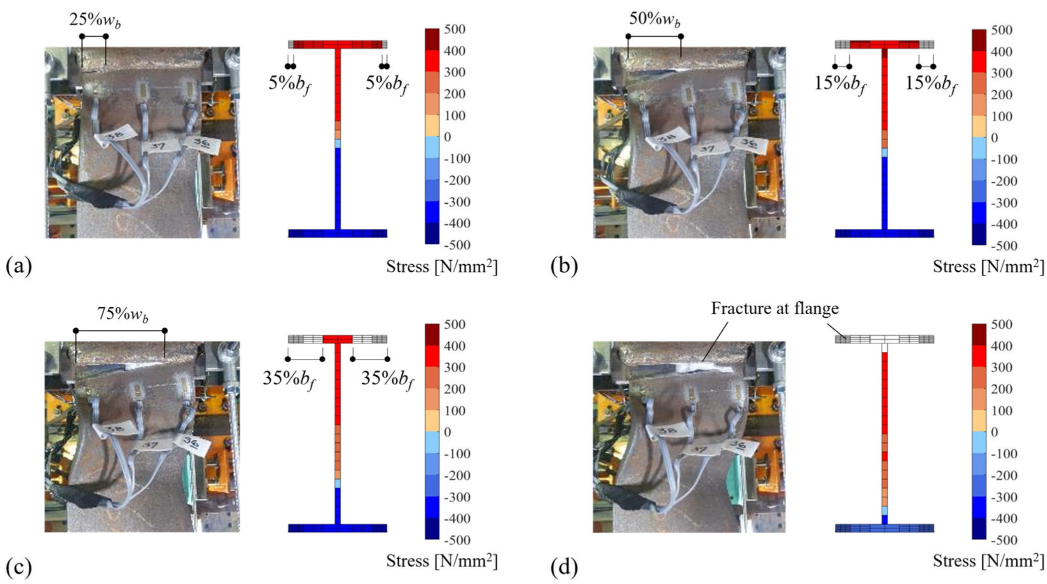

Fig 12 Comparison on failure propagation: (a) Point A; (b) Point B; (c) Point C; (d) Point D.

analysis was adopted to studied interaction effect on plastic strength. A BRB-to-Beam-to-Column joint was proposed, and it reproduced the measured responses with acceptable precision. Material models to simulated beam local buckling and low-cycle fatigue was calibrated based on a proposed beam model. Same modeling technique was verified by time history analysis of a 4-story MRF.

For studies related to panel zone, key findings are summarized below:

(1) The presented method based on equilibrium derived reasonable shear forces of panel zones, which agreed with the measured shear force and theoretical stiffness of the panel zone;

(2) The measured response of the panel zones was clearly affected by force interaction due to bidirectional loading. When the panel zone developed significant deformation and shear force in one direction, the shear strength in the orthogonal direction reduced substantially;

(3) The simple modeling of panel zone represented stiffening due to bracing connections by a short truss between the beam and column elements. After calibration from pushover analysis and selection based on the measured panel-zone deformation, the model was able to capture elasto-plastic panel-zone responses.

For studies related to beam local buckling and fatigue simulation, key findings are summarized below:

(1) With calibrated parameters of Hysteretic and Fatigue model, the beam model reproduced strength degradation at both loading sides, and the simulated fiber failure agreed with the crack propagation observed in subassemblage tests;

(2) The 4-story model of time history analysis underestimated the measured story deformation before fracture happened. With the same modeling of beam and material models, the simulation showed consistent strength degradation at the same location and same excitation with the test.

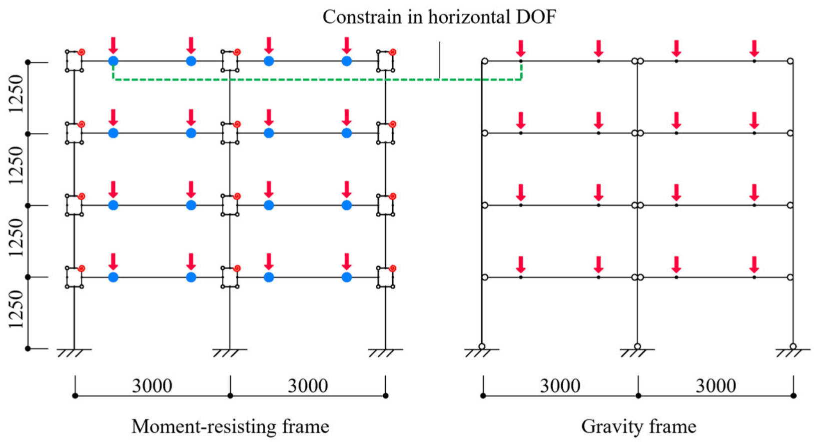

Fig 13. Numerical model of 4-story specimen

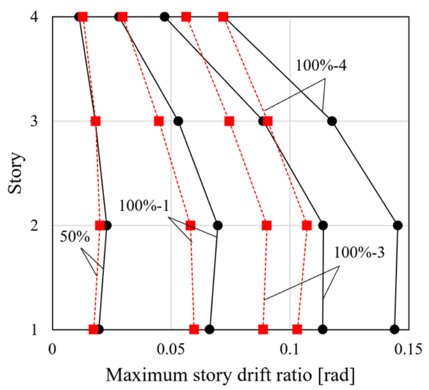

Fig 14. Maximum story drift ratio

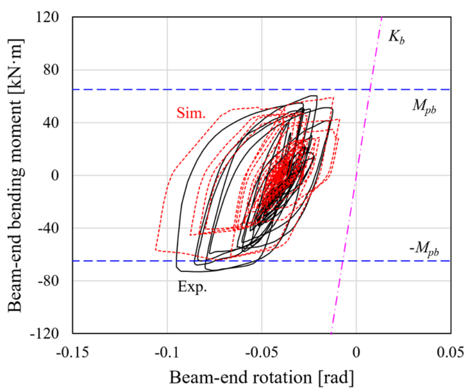

Fig 15. Beam-end bending moment vs rotation

References

[1] S. Kishiki, D. Kadono, K. Satsukawa, S. Yamada. Consideration of Composite Effects on Elasto-Plastic Behavior of Panel-Zone. *J. Struct. Constr. Eng., AIJ*, 75, 1527–1536, 2010. https://doi.org/10.3130/aijs.75.1527.

[2] *Recommendations for Design of Connections in Steel Structures*. AIJ (Architecture Institute of Japan), Japan, 2021.

[3] R. Arakida, I. Chan, Y. Koetaka. Full Plastic Strength of Square Hollow Section Panel Zone under Arbitrary Directional Shear Force. *Journal of Structural and Construction Engineering*, 84, 85–95, 2019. https://doi.org/10.3130/aijs.84.85.

[4] N. Luco, Y. Mori, Y. Funahashi, C.A. Cornell, M. Nakashima. Evaluation of Predictors of Non-Linear Seismic Demands Using “fishbone” Models of SMRF Buildings. *Earthquake Engineering and Structural Dynamics*, 32, 2267–2288, 2003. https://doi.org/10.1002/eqe.331.

[5] A. Gupta, H. Krawinkler. *Seismic Demands for Performance Evaluation of Steel Moment Resisting Frame Structures*. 1999. http://blume.stanford.edu.

[6] P. Uriz, S.A. Mahin. *Toward Earthquake-Resistant Design of Concentrically Braced Steel-Frame Structures*. 2008.